Colloidal Stochastic Resonance in Confined Geometries

Qian Zhu,[1] Yang Zhou,[1] Fabio Marchesoni,[2,3] and H. P. Zhang[1,*]

[1]*School of Physics and Astronomy and Institute of Natural Sciences, Shanghai Jiao Tong University, Shanghai 200240, China*
[2]*Center for Phononics and Thermal Energy Science, School of Physics Science and Engineering, Tongji University, Shanghai 200092, China*
[3]*Dipartimento di Fisica, Universitá di Camerino, I-62032 Camerino, Italy*

We investigate the dynamical properties of a colloidal particle in a double cavity. Without external driving, the particle hops between two free-energy minima with transition mean time depending on the system's entropic and energetic barriers. We then drive the particle with a periodic force. When the forcing period is set at twice the transition mean time, a statistical synchronization between particle motion and forcing phase marks the onset of a stochastic resonance mechanism. Comparisons between experimental results and predictions from the Fick-Jacobs theory and Brownian dynamics simulation reveal significant hydrodynamic effects, which change both resonant amplification and noise level. We further show that hydrodynamic effects can be incorporated into existing theory and simulation by using an experimentally measured particle diffusivity.

Noise is widely regarded as a disturbance in signal detection and transmission. However, quite to the contrary, an optimal amount of noise was shown to amplify the response of a nonlinear system to a weak external forcing signal [1–13]. Such a counterintuitive resonant phenomenon, known as stochastic resonance (SR), has been observed in the most diverse natural systems, ranging from physics [10], to chemistry [14], engineering [15], and biomedical sciences [16]. SR represented a paradigmatic shift in the way we think about noise in systems out of equilibrium: we realized that noise can play a constructive role in many technological applications, such as energy harvesting [17], image processing [18], and signal amplification [12].

Since its discovery in the early 1980s, SR has been studied mostly in purely energetic multistable potentials [10]. However, at the microscopic scale, the dynamics of a system is governed by its free energy, which can be dominated by entropic rather than energetic terms. For example, in soft condensed matter and in a variety of biological systems [19,20], particles are often confined to constrained geometries, such as micro- and nanofluidic devices [21–24], porous mediums [25–27], and cells [28–31], whose size and shape surely affect the SR mechanism. Burada *et al.* [13] considered the case of a Brownian particle moving in a double cavity under the action of a periodic force, oriented along the cavity axis, and a constant transverse force. They eliminated the particle's transverse degrees of freedom by introducing an effective entropic term in the Fick-Jacobs (FJ) equation [32,33] for its axial coordinate, and demonstrated that the entropic barrier corresponding to the opening connecting

the two cavities suffices to cause SR. Hereafter many theoretical and numerical studies on entropic SR in confined structures have appeared. Researchers have investigated how entropic SR depends on a variety of factors, like boundary shape [34–36], external forcing [37–39], and noise properties [40,41]; the possibility of using entropic SR for particle manipulation has also been explored [42].

As of today, a quantitative experimental demonstration of entropic SR is missing, even though detailed experimental data are urgently needed to validate theoretical assumptions and compare with numerical predictions. Here, we experimentally measure diffusion-driven transport of Brownian particles along the axis of a double cavity. In the absence of external driving, the particles switch spontaneously between two free-energy wells. Under periodic driving, SR occurs for driving periods of about twice the switching time [1–13]. Discrepancies between experimental results and predictions from the FJ theory and Brownian dynamics (BD) simulations are a measure of prominent hydrodynamic effects overlooked in the current literature; a close quantitative agreement is restored only by introducing a space-dependent diffusion function to be measured inside the cavity [22,43–47].

Experimental setup.—Our experimental setup is built on an inverted microscope stage. As shown in Fig. 1(a), a superparamagnetic colloid of radius $r = 0.25 \mu m$ is immersed in a double-well microstructure and experiences an oscillatory force in the x direction, $\tilde{F}(t)\vec{e}_x$. The force is generated by a pair of permanent magnets mounted on a linear stage, which modulates the magnets' position to control the force [48]. To generate a potential barrier [13], a third magnet was introduced, which exerts a force $-\tilde{G}\vec{e}_y$ in the y direction.

098001-1
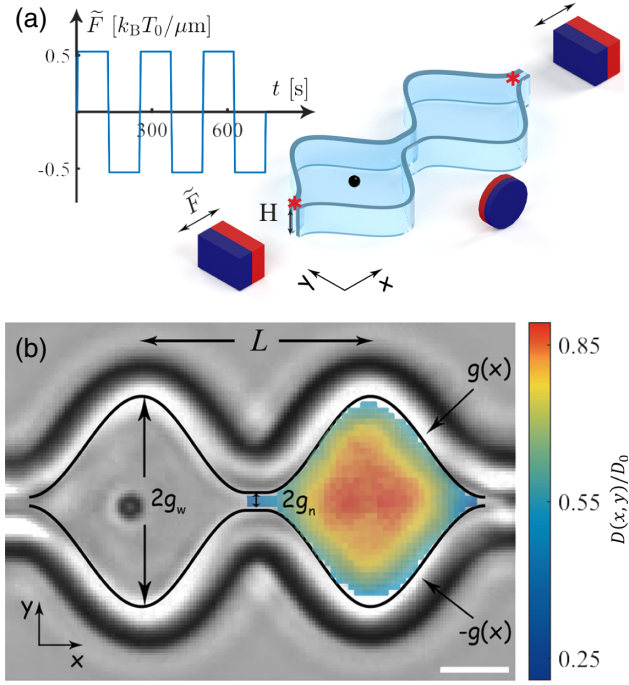
FIG. 1. (a) Schematic illustration (not to scale) of the experimental setup, including a superparamagnetic particle in a double cavity, a pair of permanent magnets on a translation stage in the x direction, and a third permanent magnet in the y direction. Oscillatory forcing in the x direction is shown in the inset. (b) Optical image of a double cavity (scale bar, 2 μm). Black solid lines, $\pm g(x)$, represent the effective boundary of the space accessible to the particle center, see Fig. S1 in SM. Geometric parameters, L, g_n, and g_w, are defined in the text. The spatially varying particle diffusivity, $D(x, y)$, is overlayed on the right half of the image; D_0 is the particle diffusivity in the open region of the cavity.

Our cavities were fabricated on a coverslip by means of a two-photon direct laser writing system. The quasi-2D cavity has a uniform height [$H = 2.7$ μm in Fig. 1(a)]. The space accessible to the particle center in the cavity has a local width $2g(x)$ along its axis x. As shown by solid lines in Fig. 1(b), $g(x)$ is given the form of an approximate cosine of period L, which then tapers off to a constant in correspondence with the bottlenecks; $g_{n(w)}$ represent its minimum(maximum) half-width, respectively [48]. We varied g_n (from 0.25 to 0.75 μm) and fixed other parameters ($L = 6.4$ μm, $g_w = 2.95$ μm) in the experiment. Particle motion in the quasi-2D cavity was recorded through a microscope. The projected particle trajectory in the $x - y$ plane was extracted from the recorded videos by standard particle tracking algorithms. Experiments were carried out at room temperature $T_0 = 297$ K.

Numerical simulation and FJ theory.—The Brownian motion of a particle with a friction coefficient γ_0 can be modeled by the Langevin equation,

$$\frac{d\vec{r}}{dt} = -G\vec{e}_y + F(t)\vec{e}_x + \sqrt{D_0}\vec{\xi}(t), \qquad (1)$$

where the first two terms on the rhs are the contributions from the external forces, $G = \tilde{G}/\gamma_0$ and $F(t) = \tilde{F}(t)/\gamma_0$, $D_0 = k_B T/\gamma_0$ is the free particle diffusivity, and $\vec{\xi}(t)$ is a 2D zero-mean Gaussian noise with correlation functions $\langle \xi_i(t)\xi_j(t') \rangle = 2\delta_{ij}\delta(t - t')$ for $i, j = x, y$. The driving force in the x direction, $\tilde{F}(t)$, is given as a square wave with an amplitude $\tilde{F}_0$ and a period T_ν, see the inset of Fig. 1(a). Particle motion in our cavity occurs mainly in the lateral direction. For such quasi-one-dimensional (1D) channels [49,50], Jacobs and Zwanzig proposed a reduced theoretical formulation [32,33]; they assumed that the transverse degrees of freedom equilibrate fast and eliminated them adiabatically by means of an approximate perturbation scheme. The FJ equation governing the probability density, $p(x, t)$, of the stochastic process of Eq. (1) reads

$$\frac{\partial}{\partial t}p(x,t) = \frac{\partial}{\partial x}\left\{ D_0 \frac{\partial p}{\partial x} + [V'(x, D_0) - F(t)]p(x,t) \right\}, \qquad (2)$$

with effective potential [20]

$$V(x, D_0) = -D_0 \ln\left[\frac{2D_0}{G}\sinh\left(\frac{Gg(x)}{D_0}\right) \right]. \qquad (3)$$

We remark that, although originally the friction coefficient, γ_0, and the particle diffusion constant, D_0, were assumed to be constant, the FJ equations (2) and (3) can be generalized for space dependent coefficients to incorporate additional boundary curvature [51–54] and hydrodynamic effects [22,46].

Particle free diffusion.—We first investigate particle diffusion in an unbiased cavity, $F(t) = 0$. The temporal record of the particle x coordinate plotted in Fig. 2(a), shows that the particle stochastically switches between two free-energy minima at $\pm x_m = \pm 3.2$ μm. Following the procedure detailed in the Supplemental Material SM [48], we identified the switching event times, t_i, marked in the figure by vertical lines; the time difference between two subsequent switching events, $\mathcal{T}(i) = t_i - t_{i-1}$, is defined as the residence time at time t_i. In Figs. 2(b) and 2(c), we plot the probability distribution of the residence times, $N(\mathcal{T})$, measured in experiments with two different cavity neck widths ($g_n = 0.25$ and 0.75 μm), with and without the y magnet (G_{on}/G_{off}). In all experiments $N(\mathcal{T})$ can be fitted by the exponential law, $N(\mathcal{T}) = (1/T_k)\exp(-(\mathcal{T}/T_k))$, with one free parameter, the Kramers time T_k [10]. Our experimental estimates of the Kramers times, reported in Figs. 2(d) and 2(e), increase sharply with decreasing neck width, g_n, or adding an energy barrier, G [13].

From the FJ equations (2) and (3), we calculated the mean first-passage time [10,22] for the particle to diffuse from $-x_m$ to x_m, which is known to return a close approximation of the Kramers time,
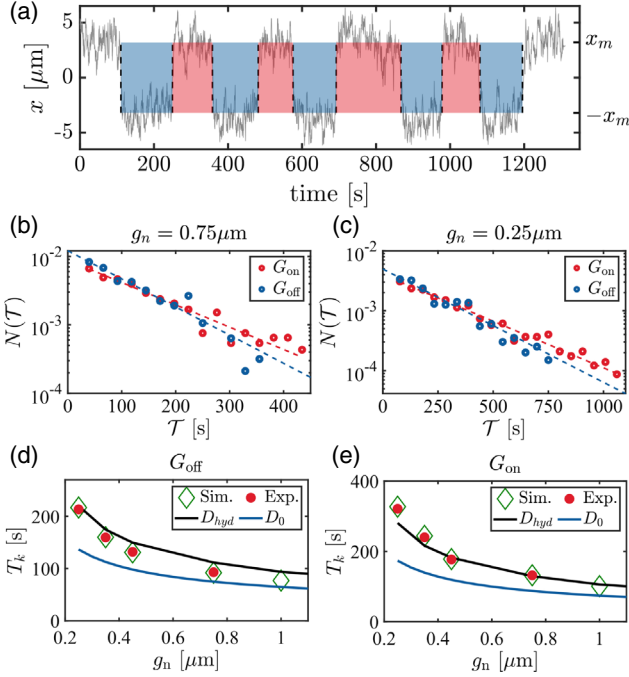
FIG. 2. Diffusion in a double cavity without periodic forcing. (a) Temporal record of the particle x coordinate. The blue(red) areas denote its residence times of the particle on the left(right) side of the cavity. (b), (c) Distribution of residence times in wide and narrow neck cavities. Experimental and fitting results are denoted by symbols and dashed lines, respectively. (d), (e) Kramers times in different cavities without, (d), and with transverse force $G = 0.55\ \mu m/s$, (e). Experimental and numerical results are represented by symbols; predictions from the FJ theory by blue (constant diffusivity, D_0) and black [measured x-dependent diffusivity, $D_{\mathrm{hyd}}(x)$] curves.

$$T_k \approx \int_{-x_{\mathrm{m}}}^{x_{\mathrm{m}}} \frac{d\chi}{\mathbb{D}(\chi)\sinh\left(\frac{Gg(\chi)}{\mathbb{D}(\chi)}\right)} \int_{-x_{\mathrm{m}}}^{\chi} \sinh\left(\frac{Gg(\zeta)}{\mathbb{D}(\zeta)}\right) d\zeta. \quad (4)$$

We have replaced the diffusion constant, D_0, in Eqs. (2) and (3) by an x-dependent particle diffusivity, which incorporates both the entropic corrections resulting from the adiabatic elimination of the transverse coordinate [51–54], and the hydrodynamic effects [22,46], that is

$$\mathbb{D}(x) = \frac{D_{\mathrm{hyd}}(x)}{[1 + g'(x)^2]^{1/3}}. \quad (5)$$

The elimination of the transverse coordinate [51–54] requires that the cavity slope cannot be significantly greater than one; see Sec. VII in the SM for further discussions. Following the approach of Ref. [22] to include hydrodynamic effects, we measured the xx component of the particle diffusivity tensor throughout the cavity, $D_x(x, y)$—examples of the spatially dependent diffusivity are reported in Figs. 1(b) and S4. The measured diffusivity $D_x(x, y)$ was

then averaged in the y direction to extract the averaged diffusivity, $D_{\mathrm{hyd}}(x)$, appearing in Eq. (5), see detailed procedure in the SM [48]. As shown by black curves in Figs. 2(d) and 2(e), Eqs. (4) and (5) yield predictions in excellent agreement with experiments. On the contrary, had we used the constant diffusivity, D_0, measured in the open part of the cavity, this approach would have worked only for cavities with wide necks, see blue curves in Figs. 2(d) and 2(e). Such a discrepancy is due to the hydrodynamic effects, which significantly suppress diffusivity in the neck region. In BD simulations, hydrodynamic effects can be reproduced by integrating the Langevin equation (1) for local friction and diffusion coefficients, $\gamma_x(x, y)$ and $D_x(x, y)$ (see SM [48] for technical details); results are shown as triangles in Figs. 2(d) and 2(e).

Stochastic resonance.—After quantifying the equilibrium dynamics, we next carried out *nonequilibrium* experiments, whereby the colloid trapped in a cavity is periodically driven by a pair of permanent magnets. In sharp contrast with the undriven cases of Figs. 2(b) and 2(c), the residence time distributions in Figs. 3(a) and 3(b) exhibit a series of peaks, centered at the odd multiples of the half-driving period, $T_n = (n - 1/2)T_\nu$, with $n = 1, 2, \ldots$ [9–11]. Under a standard two-state approximation, $N(\mathcal{T})$ can be calculated from the Langevin equation (1) [4,10]. We empirically adapted that result to our system, $N(\mathcal{T}) = N_0[1 - \frac{1}{2}(\tilde{F}_0 x_m/k_B T)^2 \cos(2\pi\mathcal{T}/T_\nu)]\exp(-(\mathcal{T}/T_k))/T_k$, where N_0 is a normalization factor and the time scale, T_k, is determined through Eq. (4) [6,10]. As illustrated in Figs. 3(a) and 3(b), predictions of the equation above agree fairly closely with experiments and BD simulations without any additional fitting parameter.

To quantify the statistical synchronization between periodic forcing and well switching, we integrated the area under the first $N(\mathcal{T})$ peak at $\mathcal{T} = T_\nu/2$: $P_1 = \int_{T_\nu/4}^{3T_\nu/4} N(\mathcal{T})d\mathcal{T}$ [the red area under the first peak in Figs. 3(a) and 3(b)]. Our experimental data for P_1, plotted in Fig. 3(c), exhibit a broad peak centered around $T_\nu = 2T_k$, which is consistent with many previous results [11,55].

To further test the FJ theory, we numerically integrated Eq. (2) [56–58] and used the probability distribution, $p(x, t)$, to compute the time-dependent average, $\langle x(t)\rangle = \int x p(x, t)dx$. Through an appropriate Fourier expansion [13], we extracted the amplitude, M_1, of the first harmonic of $\langle x(t)\rangle$ at the driving frequency, $\nu = 1/T_\nu$. Accordingly, the spectral amplification, η, defined as the ratio of the power stored in the system response and the power of the external force, $F(t)$, at frequency ν, could be computed as $\eta = [M_1/F_0]^2$. The spectral amplification increases with the driving period as shown in Fig. 3(c); experimental, theoretical, and simulation data agree again with one another [9,55].
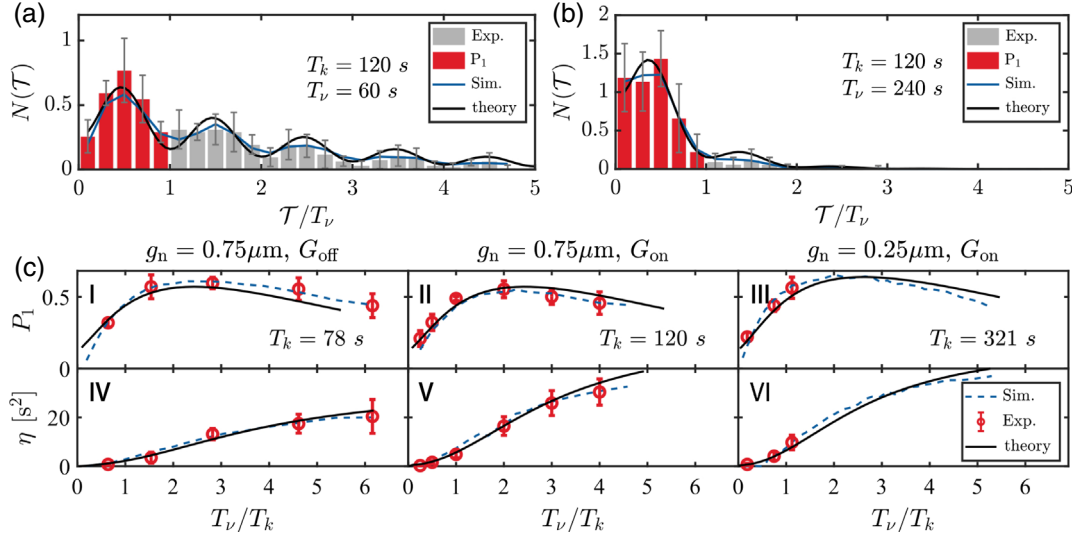
FIG. 3. (a), (b) Normalized residence time distributions from experiments, theory, and simulations, for two forcing periods, $T_\nu = 60$ s (a) and $T_\nu = 240$ s (b), in a wide neck cavity ($g_n = 0.75$ μm) with Kramers time $T_k = 120$ s. The red vertical bars represent the area of the first peak, P_1, from the experiments. (c) First peak of the residence time distributions, P_1 (I-III), and spectral amplification, η (IV-VI), plotted versus the normalized forcing period, T_ν / T_k, under three different experimental conditions. Transverse force $G = 0.55$ μm/s was used for experiments of the middle and right columns in (c) (G_{on}). Error bars represent standard errors from experimental measurements.

The results of Fig. 3 prove that we can reliably account for hydrodynamic effects in *nonequilibrium* situations by means of a suitable space dependent diffusion function. This gives us a powerful tool to investigate SR under the influence of strong hydrodynamic effects. To that end, we performed BD simulations [Eq. (S3) in SM] for the spatially varying friction coefficient, $\gamma_x(x, y)$, computed with COMSOL, and different temperatures, T, to tune the noise level. From the BD particle trajectories, we computed the spectral amplification, η. In Fig. 4, we plot η as a function of the noise level, quantified here by the thermal energy, $k_B T$. In all cases, a resonant peak of η is observed at some intermediate value of $k_B T$, which means that SR occurs also in the presence of strong hydrodynamic effects, and the FJ theory with $D_{hyd}(x)$ yields predictions (solid curves) in excellent agreement with BD simulations. The $\eta(k_B T)$ curves displayed in Fig. 4 clearly show that (i) the resonance peak is more pronounced as the forcing frequency decreases [Fig. 4(a)]; (ii) the maximal amplification is enhanced by lowering the intensity of the transverse force, G [Fig. 4(b)]; and (iii) both the peak amplification and the optimal SR noise level increase with decreasing the forcing amplitude, F_0. Results in Figs. 4(a)–4(c) are qualitatively similar to those earlier obtained for systems with constant diffusivity [10,13]. The data in Fig. 4(d) show how hydrodynamic effects *quantitatively* affect the SR behavior overall. For the wide neck cavity ($g_n = 0.75$ μm), the spatial modulation of $\gamma_x(x, y)$ is negligible; hence, FJ predictions with $D_{hyd}(x)$ (solid curve) and D_0 (dashed curve) are in excellent agreement with the BD simulation output. On the contrary, for the narrow neck cavity

($g_n = 0.25$ μm), where hydrodynamic effects are known to be strong, the FJ theory with constant diffusivity, D_0, would predict higher amplification peaks and lower optimal noises.
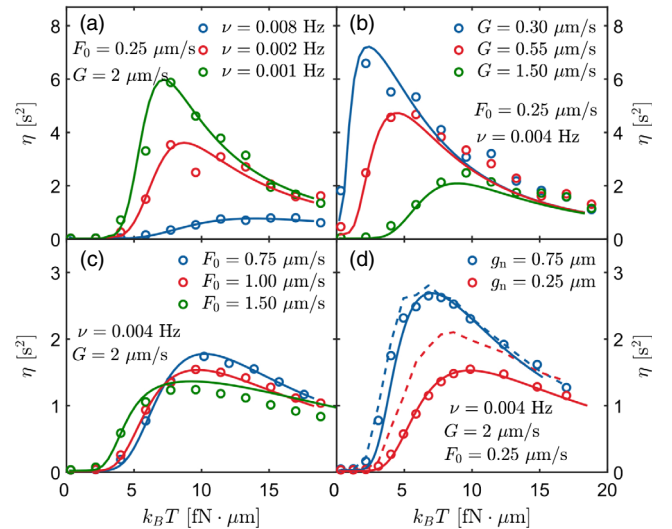
FIG. 4. Dependence of the spectral amplification, η, on the noise level, $k_B T$, for different experimental conditions, (a) driving frequency ν, (b) transverse force G, (c) driving amplitude F_0, (d) cavity minimum half-width g_n. Circles and solid lines represent results, respectively, from BD simulation and FJ theory with spatially varying friction coefficient. The dashed curves in (d) are obtained from the FJ theory with constant diffusivity, D_0, in Eq. (5). The narrow neck cavity ($g_n = 0.25$ μm) was used in (a)–(c).

Conclusion.—We have experimentally investigated colloidal transport in a double cavity. When a particle is subjected to a periodic force with a period twice the Kramers time, the particle's motion is statistically synchronized with the drive. This provides a direct demonstration of the entropic SR mechanism theoretically predicted in Ref. [13]. We further observed that strong hydrodynamic effects in cavities with tight constrictions can quantitatively affect the optimal SR parameters. We successfully reproduced such hydrodynamic effects in the nonequilibrium BD simulations and FJ theory by introducing a space dependent friction coefficient to be either measured from experiments or computed from hydrodynamic models. Our results confirm that the proposed generalization of the FJ theory is indeed a predictive tool to study driven transport in tightly constrained geometries with strong entropic and hydrodynamic effects.

---

*hepeng_zhang@sjtu.edu.cn

[1] R. Benzi, A. Sutera, and A. Vulpiani, J. Phys. A **14**, L453 (1981).

[2] C. Nicolis, Tellus **34**, 1 (1982).

[3] S. Fauve and F. Heslot, Phys. Lett. **97A**, 5 (1983).

[4] McNamara and Wiesenfeld, Phys. Rev. A **39**, 4854 (1989).

[5] L. Gammaitoni, F. Marchesoni, E. Menichella-Saetta, and S. Santucci, Phys. Rev. Lett. **62**, 349 (1989).

[6] T. Zhou, F. Moss, and P. Jung, Phys. Rev. A **42**, 3161 (1990).

[7] P. Jung and P. Hanggi, Phys. Rev. A **44**, 8032 (1991).

[8] J. K. Douglass, L. Wilkens, E. Pantazelou, and F. Moss, Nature (London) **365**, 337 (1993).

[9] L. Gammaitoni, F. Marchesoni, and S. Santucci, Phys. Rev. Lett. **74**, 1052 (1995).

[10] L. Gammaitoni, P. Hänggi, P. Jung, and F. Marchesoni, Rev. Mod. Phys. **70**, 223 (1998).

[11] D. Babic, C. Schmitt, I. Poberaj, and C. Bechinger, Europhys. Lett. **67**, 158 (2004).

[12] R. L. Badzey and P. Mohanty, Nature (London) **437**, 995 (2005).

[13] P. S. Burada, G. Schmid, D. Reguera, M. H. Vainstein, J. M. Rubi, and P. Hänggi, Phys. Rev. Lett. **101**, 130602 (2008).

[14] P. Hanggi, ChemPhysChem **3**, 285 (2002).

[15] Z. J. Qiao, Y. G. Lei, and N. P. Li, Mech. Syst. Signal Process **122**, 502 (2019).

[16] M. D. McDonnell and D. Abbott, PLoS Comput. Biol. **5**, e1000348 (2009).

[17] C. R. McInnes, D. G. Gorman, and M. P. Cartmell, J. Sound Vib. **318**, 655 (2008).

[18] O. van der Groen and N. Wenderoth, J. Neurosci. **36**, 5289 (2016).

[19] P. Hänggi and F. Marchesoni, Rev. Mod. Phys. **81**, 387 (2009).

[20] P. S. Burada, P. Hänggi, F. Marchesoni, G. Schmid, and P. Talkner, ChemPhysChem **10**, 45 (2009).

[21] S. Matthias and F. Muller, Nature (London) **424**, 53 (2003).

[22] X. Yang, C. Liu, Y. Li, F. Marchesoni, P. Hänggi, and H. P. Zhang, Proc. Natl. Acad. Sci. U.S.A. **114**, 9564 (2017).

[23] M. J. Skaug, C. Schwemmer, S. Fringes, C. D. Rawlings, and A. W. Knoll, Science **359**, 1505 (2018).

[24] C. Schwemmer, S. Fringes, U. Duerig, Y. K. Ryu, and A. W. Knoll, Phys. Rev. Lett. **121**, 104102 (2018).

[25] B. Berkowitz, A. Cortis, M. Dentz, and H. Scher, Rev. Geophys. **44**, RG2003 (2006).

[26] D. Wang, H. Wu, L. Liu, J. Chen, and D. K. Schwartz, Phys. Rev. Lett. **123**, 118002 (2019).

[27] H. Wu and D. K. Schwartz, Acc. Chem. Res. **53**, 2130 (2020).

[28] H.-X. Zhou, G. Rivas, and A. P. Minton, Annu. Rev. Biophys. **37**, 375 (2008).

[29] P. C. Bressloff and J. M. Newby, Rev. Mod. Phys. **85**, 135 (2013).

[30] F. Hofling and T. Franosch, Rep. Prog. Phys. **76**, 046602 (2013).

[31] A. Agrawal, Z. C. Scott, and E. F. Koslover, Annu. Rev. Biophys. **51**, 247 (2022).

[32] M. Jacobs, *Diffusion Processes* (Springer, New York, 1967).

[33] R. Zwanzig, J. Phys. Chem. **96**, 3926 (1992).

[34] P. S. Burada, G. Schmid, D. Reguera, J. M. Rubi, and P. Hänggi, Eur. Phys. J. B **69**, 11 (2009).

[35] P. K. Ghosh, F. Marchesoni, S. E. Savel'ev, and F. Nori, Phys. Rev. Lett. **104**, 020601 (2010).

[36] R. Mei, Y. Xu, Y. Li, and J. Kurths, Phil. Trans. R. Soc. A **379**, 20200230 (2021).

[37] P. S. Burada, G. Schmid, D. Reguera, J. M. Rubi, and P. Hänggi, Europhys. Lett. **87**, 50003 (2009).

[38] H. Ding, H. Jiang, and Z. Hou, J. Chem. Phys. **143**, 244119 (2015).

[39] L. C. Du, W. H. Yue, J. H. Jiang, L. L. Yang, and M. M. Ge, Phil. Trans. R. Soc. A **379**, 20200228 (2021).

[40] L. Zhao, X. Q. Luo, D. Wu, S. Q. Zhu, and J. H. Gu, Chin. Phys. Lett. **27**, 040503 (2010).

[41] J. Z. Xu and X. Q. Luo, Chin. J. Phys. **63**, 382 (2020).

[42] N. Shi and V. M. Ugaz, Phys. Rev. E **89**, 012138 (2014).

[43] J. Happel and H. Brenner, *Low Reynolds Number Hydrodynamics* (Prentice Hall, Englewood Cliffs, NJ, 1965).

[44] W. M. Deen, AIChE J. **33**, 1409 (1987).

[45] S. L. Dettmer, S. Pagliara, K. Misiunas, and U. F. Keyser, Phys. Rev. E **89**, 062305 (2014).

[46] K. Misiunas, S. Pagliara, E. Lauga, J. R. Lister, and U. F. Keyser, Phys. Rev. Lett. **115**, 038301 (2015).

[47] X. Yang, Q. Zhu, C. Liu, W. Wang, Y. Li, F. Marchesoni, P. Hänggi, and H. P. Zhang, Phys. Rev. E **99**, 020601(R) (2019).

[48] See Supplemental Material at http://link.aps.org/supplemental/10.1103/PhysRevLett.129.098001 for detailed experimental procedure, additional experimental and numerical results, and description of Brownian dynamics model (2020).

[49] B. Hille, *Ion Channels of Excitable Membranes* (Sinauer Associates, Sunderland, MA, 2001).

[50] M. Wanunu, T. Dadosh, V. Ray, J. M. Jin, L. McReynolds, and M. Drndic, Nat. Nanotechnol. **5**, 807 (2010).

[51] D. Reguera and J. M. Rubi, Phys. Rev. E **64**, 061106 (2001).

[52] P. Kalinay and J. K. Percus, Phys. Rev. E **74**, 041203 (2006).

[53] D. Reguera, G. Schmid, P. S. Burada, J. M. Rubi, P. Reimann, and P. Hänggi, Phys. Rev. Lett. **96**, 130603 (2006).

[54] R. Verdel, L. Dagdug, A. M. Berezhkovskii, and S. M. Bezrukov, J. Chem. Phys. **144**, 084106 (2016).

[55] L. Gammaitoni, F. Marchesoni, and S. Santucci, Phys. Lett. A **195**, 116 (1994).

[56] P. Hänggi, Helv. Phys. Acta **51**, 183 (1978).

[57] O. Farago and N. Gronbech-Jensen, Phys. Rev. E **89**, 013301 (2014)-01.

[58] N. Bruti-Liberati and E. Platen, Stoch. Dyn. **08**, 561 (2008).